Supplementary material

A. Galerkin model (GK) equations

All the derivations of the mathematical models are carried out using the computer software Mathematica™. The detailed derivation of the GK models is prepared in Mathematica™ notebook format, i.e. *GK.nb*, which is included in the current supplementary material folder.

Different degree of polynomial approximation of GK models can be generated by specifying the K value at the beginning of the code. The full expression of the pressure field corresponding to equation (2.32) in the main body of the paper can be found by running the following line in the code:

```
p=(\[Rho]*g*(1-\[Sigma])+\[Rho]*pnh)/sigmaz;   (* PRESSURE FIELD *) .
```

Finally, the resulting equations consist of one depth-integrated continuity equation, which always remains the same regardless of the K value, and K number of weighted horizontal momentum equations. These will show up in the code by uncommenting the following lines:

```
Print[Ht];

Do[Print[Collect[-Subscript[XEQ, i],_[x,t],Simplify]],{i,1,K,1}];
```

An example of the $G2$ model is provided in *G2.pdf* file.

B. Subdomain model (SK) equations

Similar to the Galerkin model (GK), the derivation of the subdomain models (SK) are prepared in a notebook file, i.e. *SK.nb*.

Different degree of polynomial approximation of SK models can be generated by specifying the K value in the beginning of the code. $(K-1)$ number of free parameters are denoted as $(c_1, c_2, ...c_{K-1})$ in the code, in which $c_0 = 1$ and $c_K = 1$.

Similarly, the full expression of the pressure field corresponding to equation (2.44) in the main body of the paper can be found by running the following line in the code:

```
p=(\[Rho]*g*(1-\[Sigma])+\[Rho]*pnh)/sigmaz;   (* PRESSURE FIELD *) .
```

Finally, the resulting equations consist of one depth-integrated continuity equation and K number of weighted horizontal momentum equations. These will show up in the code by uncommenting the following lines:

```
Print[Ht];

Do[Print[Collect[-Subscript[XEQ, i],_[x,t],Simplify]],{i,1,K,1}];
```

We remark that the free parameters, $(c_1, c_2, ...c_{K-1})$, are kept undetermined in the equations derived above. An example of the $S2$ model is provided in *S2.pdf* file.

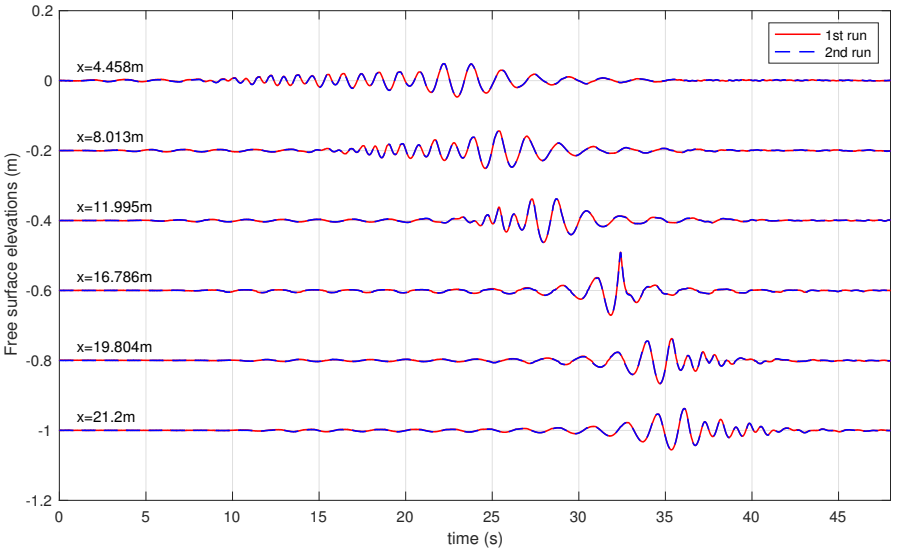

FIGURE D1. Comparison of measured free surface elevations between two separated runs. The still water level is shifted by every $-0.2m$ for better visualization.

C. Wave properties

The full expressions of linear wave properties are prepared in MATLAB® function format, i.e., *GK_linear.m* and *SK_linear.m*. These two functions contain expressions of various linear wave properties mentioned in the main body of the paper, including linear wave phase velocity, group velocity, and linear shoaling gradient. The main program *linear_main.m* can be used to call these two functions to generate the figure for comparison, which corresponds to figure 2 in the main body of the paper.

Similarly, nonlinear properties of both GK and SK models are prepared in functions, *GK_nonlinear.m* and *SK_nonlinear.m*. The main program *nonlinear_main.m* can be used to generate the figure for comparison, which corresponds to figure 5 in the main body of the paper.

D. Supplementary materials for new self-focusing wave package experiments at NUS (§4.4)

Figure D1 shows the comparison of measured free surface elevations between two separated runs for case A1. We observe that red lines and blue lines are overlapped, meaning that the wavemaker is highly repeatable.

In the following part, the comparisons of case A2 and B1 in the self-focusing wave package experiments at NUS (§4.4 of the main body of the paper) are presented.

The wave components in the wave package A2 follows a constant wave steepness distribution, and all these wave components fall into the deep water regime ($kd \approx 3.28$ to 10.47). Because of the large kd value involved in this case, we used $S5$ model to carry out the numerical simulation with $\Delta x = 0.03m$ and $\Delta t = 0.025s$. Figure D2, D3, and D4 show the comparisons between the numerical results and experimental data for the free surface elevations together with the amplitude spectra, horizontal velocity and vertical velocity time series. Quite good agreements are achieved for all gauges. As waves are

in deep water conditions, the decay of the velocity magnitude with respect to depth is quite obvious as shown in figure D3 and D4. Similar recurrence pattern of the spectral evolution is also found, which has been discussed in the main body of the paper (§4.4).

The incident wave package of case B1 follows a constant amplitude distribution, in which the wave components fall into finite water depth to deep water ($kd \approx 1.12$ to 8.15). We again use $S5$ model to perform the numerical simulations with $\Delta x = 0.03m$ and $\Delta t = 0.025s$. Figure D5, D6, and D7 show the comparisons between the numerical results and experimental data for the free surface elevations together with the amplitude spectra, horizontal velocity and vertical velocity time series. Good agreements are obtained for both the free surface elevations and velocity time series. The generation of higher harmonic waves is obvious at the gauge located at $x = 15.27m$ with noticeable wave components appearing at $4Hz$, although the highest frequency wave in the incident wave package is only $1.5Hz$. Moreover, the recurrence phenomena that these newly-generated higher harmonic waves revert back to the initial stage during the de-focusing phase is also found in the case.

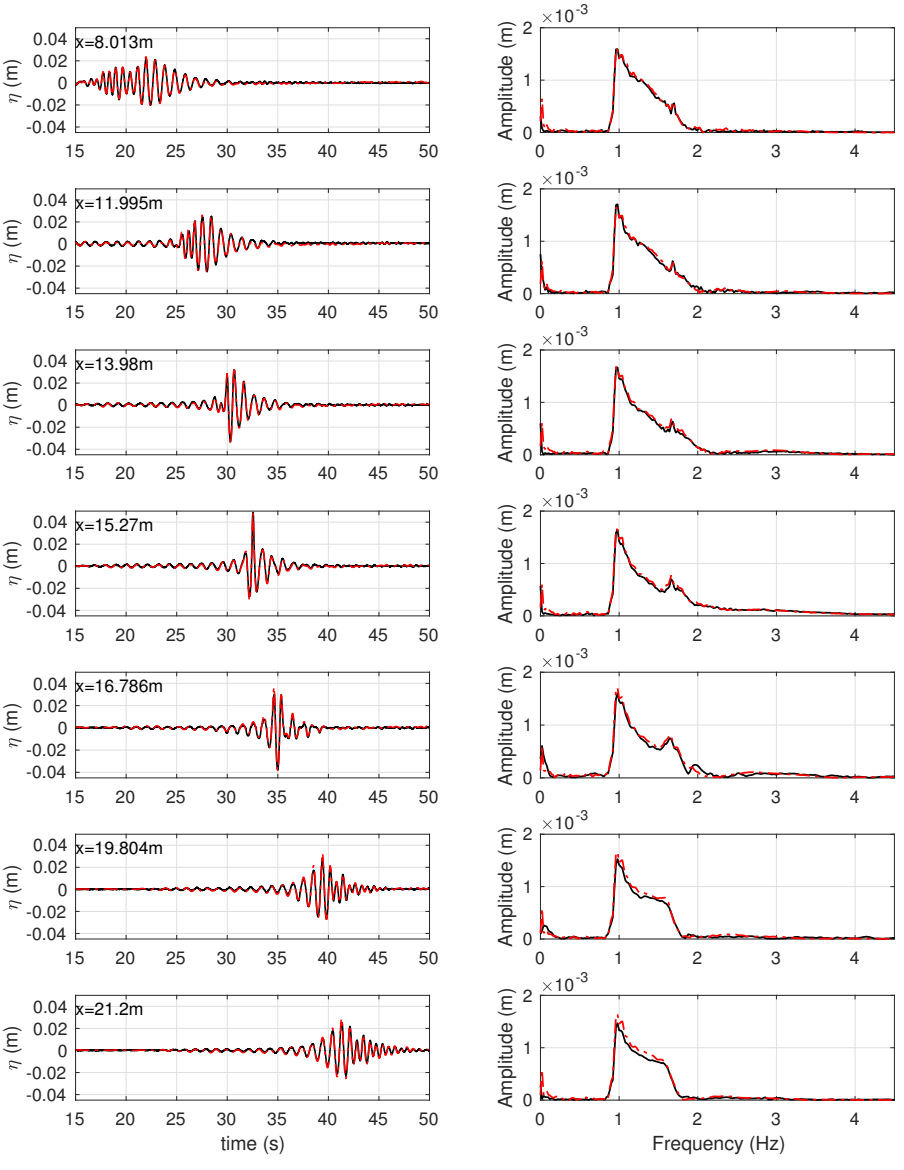

FIGURE D2. Comparisons of surface elevation time series and corresponding amplitude spectra between experimental data (black) and numerical results ($S5$ model: red dash-dotted) for case A2.

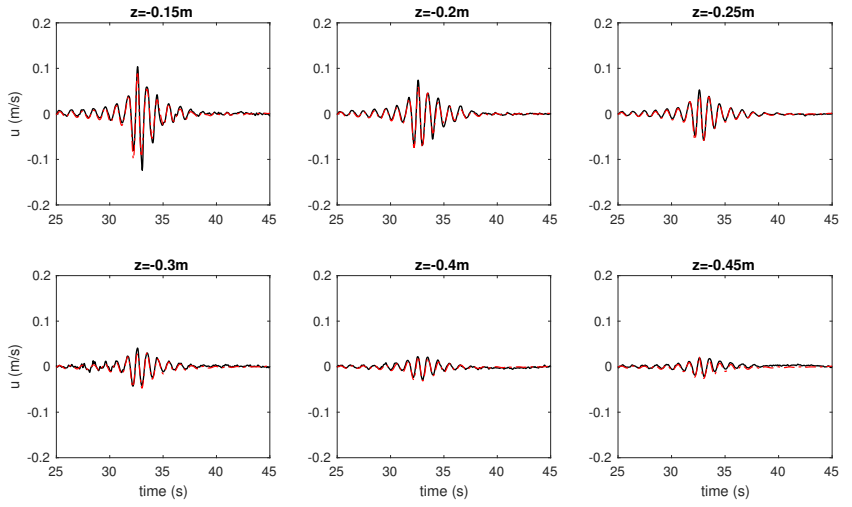

FIGURE D3. Comparisons of horizontal velocity in the water column (at $x = 15.27m$) between experimental data (black) and numerical results ($S5$ model: red dash-dotted) for case A2.

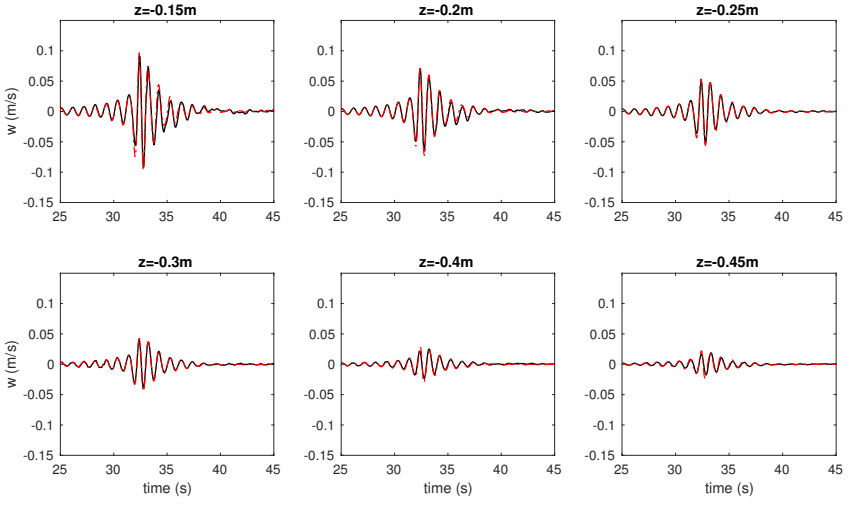

FIGURE D4. Comparisons of vertical velocity in the water column (at $x = 15.27m$) between experimental data (black) and numerical results ($S5$ model: red dash-dotted) for case A2.

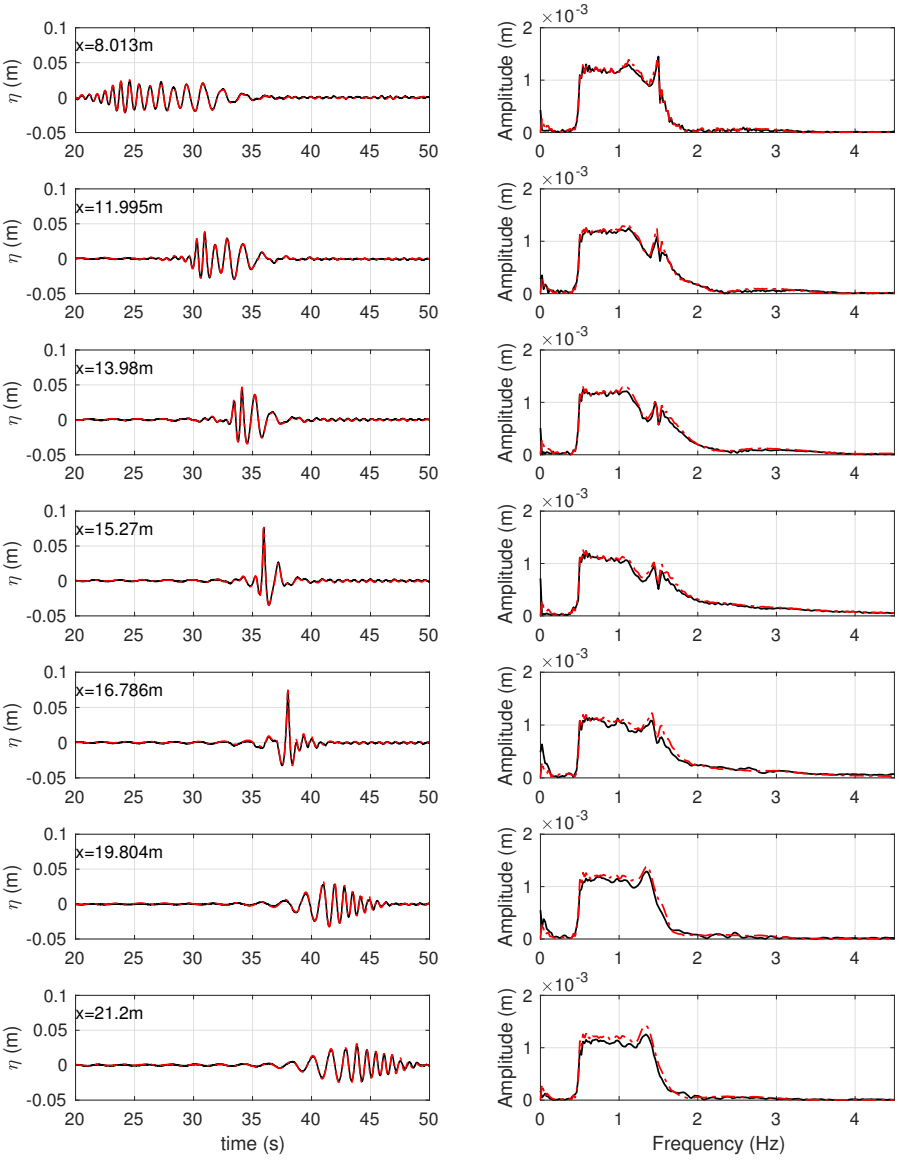

FIGURE D5. Comparisons of surface elevation time series and corresponding amplitude spectra between experimental data (black) and numerical results ($S5$ model: red dash-dotted) for case B1.

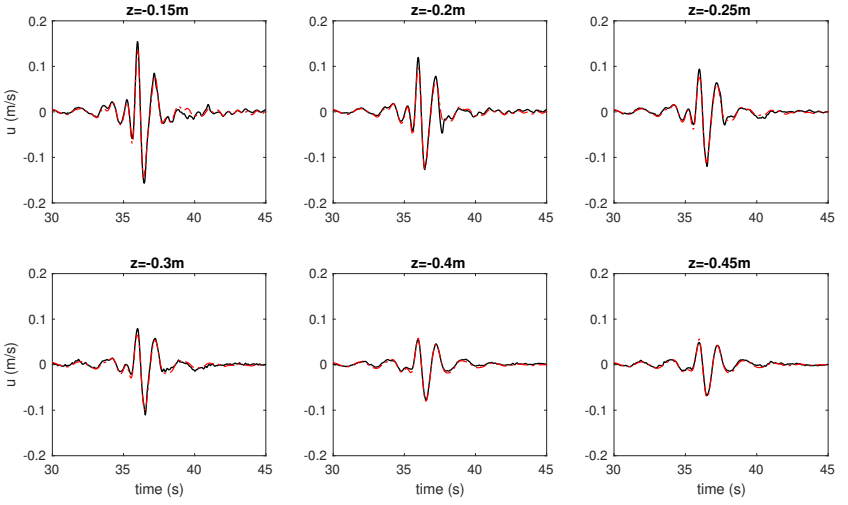

FIGURE D6. Comparisons of horizontal velocity in the water column (at $x = 15.27m$) between experimental data (black) and numerical results ($S5$ model: red dash-dotted) for case B1.

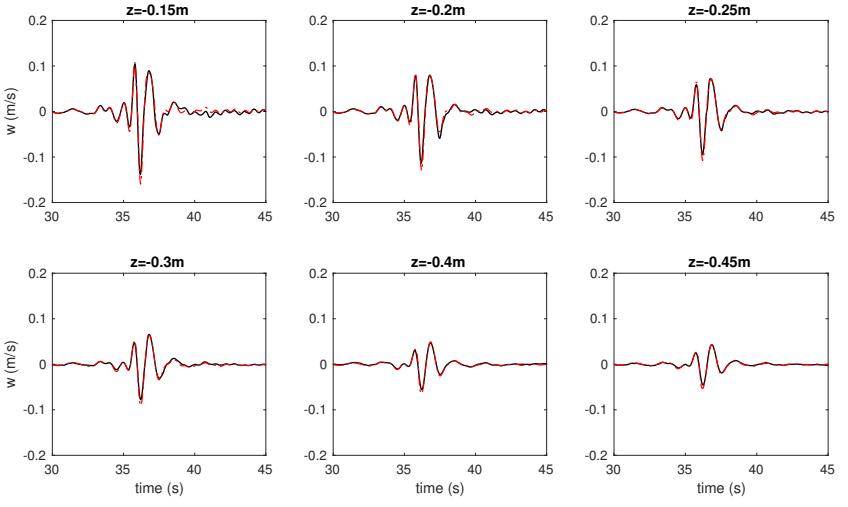

FIGURE D7. Comparisons of vertical velocity in the water column (at $x = 15.27m$) between experimental data (black) and numerical results ($S5$ model: red dash-dotted) for case B1.